# Effects of Intercalated Anions on the Interfacial Oxygen Evolution Activity and Selectivity of $NiFe(OH)_2$ Nanosheet Array Electrodes for Seawater Electrolysis

Fengyan Xiao[1]*, Fangfang Liu[2], Qin Xing[1], Runlai Jiang[3], Yangjing Liu[3], Jiaxing Ge[3], Haofeng Yan[3], Jianwei Ren[4], Hui Wang[3*]

[1]Yantai Key Laboratory of Anti-corrosion and Anti-fouling for Marine Engineering Equipment, YantaiVocational College, Yantai, Shandong Province 264670, China

[2]Shandong Engineering Research Center of New Energy Materials and Devices, Weifang University of Science and Technology, Weifang 262700, China

[3]College of Chemical Engineering, Qingdao University of Science and Technology, Qingdao, 266042, China

[4]Department of Chemical Engineering, University of Pretoria, cnr Lynnwood Road and Roper Street, Hatfield 0028, South Africa

*Corresponding author: hxzhicheng@163.com (F. Xiao); wangh@qust.edu.cn (H. Wang).

## 1. Chemicals

Iron(III) nitrate ($Fe(NO_3)_3$, ≥98.5%), nickel(II) nitrate ($Ni(NO_3)_2$, ≥98.5%), and carbon cloth (CC; Taiwan Carbon Energy Technology Co., thickness 0.35 mm, areal density 134 $g \cdot m^{-2}$, sheet resistance 1.67 $m\Omega \cdot cm^2$) were used as received. Deionized water was employed throughout the experiments.

## 2. Pretreatment of Carbon Cloth

Carbon cloth (CC) pieces with dimensions of 4 × 6 cm were placed in a PTFE-lined autoclave containing 50 mL of 65% nitric acid. The autoclave was heated at 120 °C for

8 hours to modify the surface. After treatment, the CC samples were thoroughly rinsed with deionized water and dried in an oven at 60 °C before further use.

**3. Investigation of OER Selectivity**

The oxygen evolution selectivity of the electrodes was evaluated in a three-electrode configuration using real seawater as the electrolyte. A constant current density of 100 $mA \cdot cm^{-2}$ was applied for 30 minutes, with a platinum mesh serving as the counter electrode and a saturated Hg/HgO electrode as the reference. After electrolysis, 10 mL of the anodic solution was collected, and 15 mL of 0.5 M KI solution was added to induce a color change. The appearance of a yellow-brown color indicated the presence of hypochlorous acid (HOCl) in the solution. The HOCl concentration was then determined by titration with 0.02 M sodium thiosulfate: initially, titration proceeded until the solution turned light yellow, followed by addition of 1% starch solution to facilitate accurate endpoint detection as the color disappeared. The volume of sodium thiosulfate consumed was used to calculate the hypochlorite concentration using the following equation:

$$n_{OCl^-} = (V_{Thio} \cdot C_{Thio}) / V_{Sample} \cdot V_{total}$$

Where, $n_{OCl^-}$ is the molar amount of hypochlorite ion; $V_{Thio}$ is the volume of sodium thiosulfate consumed during the titration;； $C_{Thio}$ is the molar concentration of sodium thiosulfate; $V_{Sample}$ denotes the volume of the anolyte to be titrated; $V_{total}$ is the total volume of the anolyte.

**4. Physical Characterization**

The morphology of the samples was examined using scanning electron microscopy (SEM). The crystalline structure was analyzed by X-ray diffraction (XRD) over a 2θ range of 5–90° with a scan rate of 5°·min$^{-1}$. The electronic structure and elemental composition of the synthesized materials were further investigated using X-ray photoelectron spectroscopy (XPS).

**5. Electrochemical Characterization**

The electrochemical performance of the samples was assessed using a standard three-electrode configuration on a CHI 760E electrochemical workstation. Working electrodes consisted of X-$MnO_2$/CC pieces (1 × 1 cm), with a graphite rod as the counter electrode and a Hg/HgO electrode as the reference. Two electrolytes—1 M KOH and natural seawater—were employed for comparison. Prior to testing, the electrode surfaces were cleaned and activated by cyclic voltammetry (CV) scans at 50 mV·s$^{-1}$ within a potential window of −1 to 0.2 V vs. Hg/HgO until successive CV cycles overlapped, ensuring stable surface conditions. Linear sweep voltammetry (LSV) for the OER, with 90% iR compensation, was conducted at a scan rate of 5 mV·s$^{-1}$. Potentials were converted to the reversible hydrogen electrode (RHE) scale using:

$$E_{\mathrm{RHE}} = E_{\mathrm{Hg/HgO}} + 0.059 \times \mathrm{pH} + 0.098$$

OER overpotentials (η) were calculated as:

$$\eta(\mathrm{V}) = E_{\mathrm{RHE}} - 1.23$$

Tafel slopes were derived from polarization curves by plotting η against the logarithm of the current density (j) according to the Tafel equation:

$$\eta = b\log j + a$$

where $b$ is the Tafel slope. Electrochemically active surface areas (ECSA) were estimated from the double-layer capacitance ($C_{dl}$) determined at different

CV scan rates within a non-Faradaic potential window of −0.2 to −0.1 V vs. Hg/HgO. Electrochemical impedance spectroscopy (EIS) was performed at 10 mA·cm$^{-2}$ over a frequency range of 0.01 Hz to 100 kHz to evaluate interfacial charge-transfer resistance.

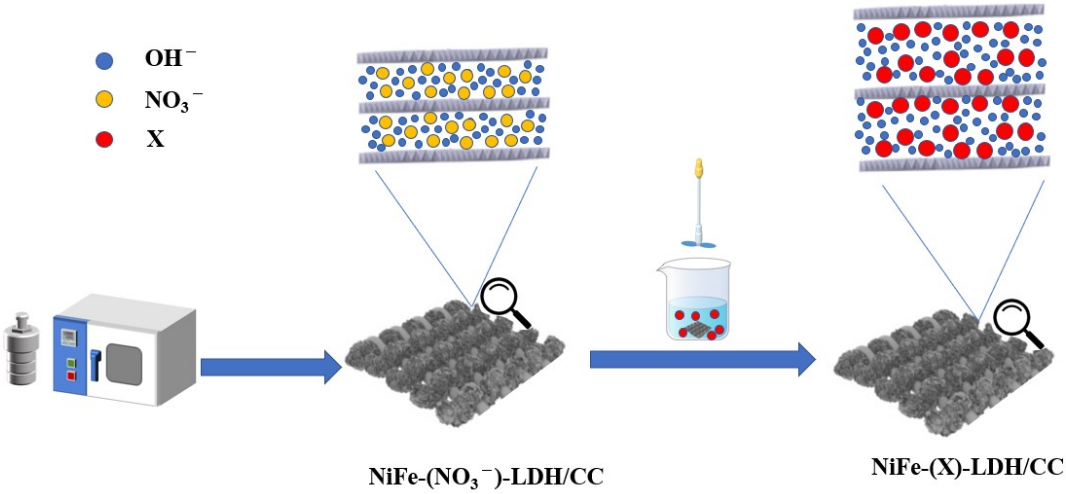


**Figure S1** Schematic illustration of the formation of NiFe-(X)-LDH/CC on carbon cloth.

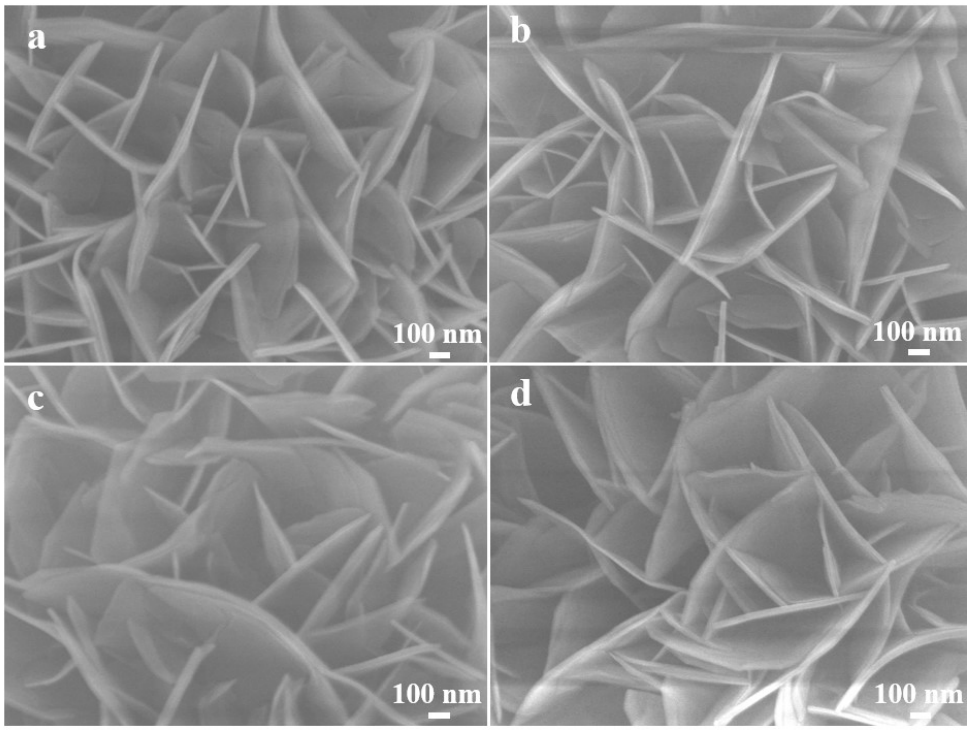

**Figure S2** SEM images of samples: (a) NiFe-($NO_3^-$)-LDH/CC; (b) NiFe-($H_2PO_2^-$)-LDH/CC; (c) NiFe-($SO_4^{2-}$)-LDH/CC; (d) NiFe-($CO_3^{2-}$)-LDH/CC

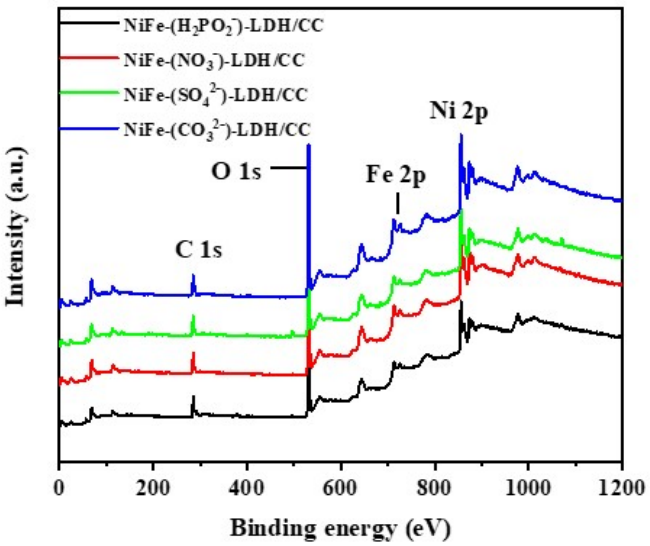


**Figure S3.** Survey XPS spectrum of NiFe-($H_2PO_2^-$)-LDH/CC,NiFe-($NO_3^-$)-LDH/CC, NiFe-($SO_4^{2-}$)-LDH/CC and NiFe-($CO_3^{2-}$)-LDH/CC

**Table S1.** The atomic percentage of each element obtained from XPS survery spectrum of the four samples.

| Atom percentage / sample | Ni% | Fe% | P/S/N/-- % | C% | O% |
|---|---|---|---|---|---|
| NiFe-($H_2PO_2^-$)-LDH/CC | 17.53 | 4.65 | 0.51 | 24.95 | 52.26 |
| NiFe-($NO_3^-$)-LDH/CC | 17.62 | 5.81 | 0.59 | 22.96 | 53.02 |
| NiFe-($SO_4^-$)-LDH/CC | 17.36 | 5.80 | 0.48 | 24.1 | 52.26 |
| NiFe-($CO_3^-$)-LDH/CC | 15.02 | 4.99 | ---- | 27.82 | 52.17 |

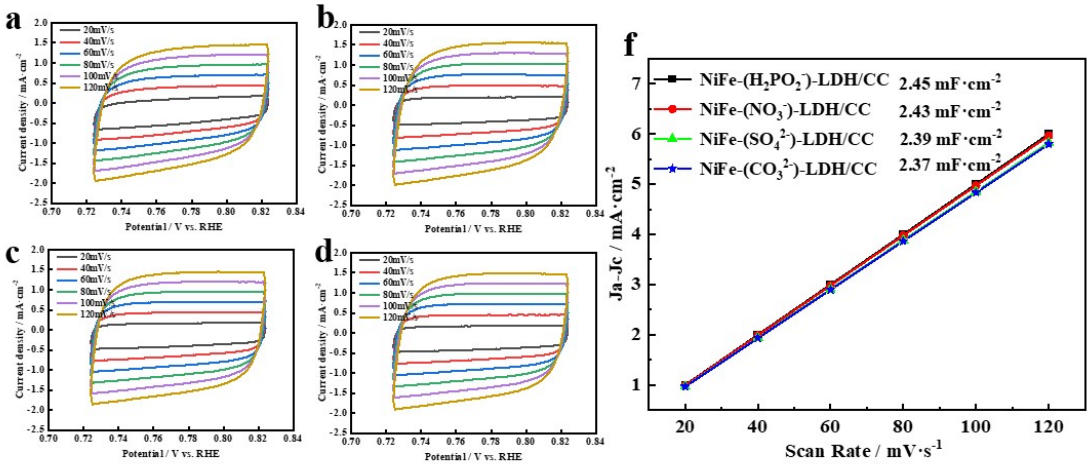


**Figure S4.** Cyclic voltammetry (CV) curves of NiFe-LDH/CC electrodes intercalated with different anions at various scan rates in 1.0 M KOH solution: (a–d) NiFe–($H_2PO_2^-$)–LDH/CC and other samples; (f) comparison of NiFe–($H_2PO_2^-$)–LDH/CC with the other catalysts.

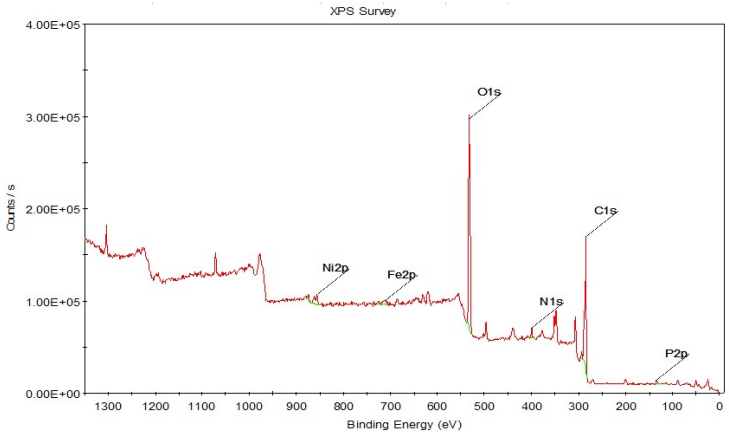


**Figure S5.** Survey XPS spectrum of NiFe-($H_2PO_2^-$)-LDH/CC after stable test.

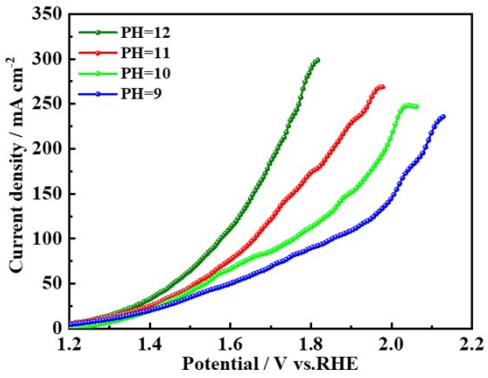


**Figure S6.** OER LSVs of the NiFe-($H_2PO_2^-$)-LDH/CC electrode in alkaline seawater with different pH values (pH = 9, 10, 11, 12).

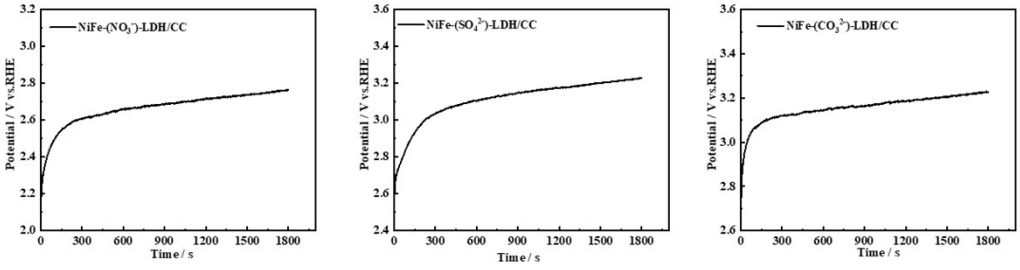


**Figure S7.** OER Constant current curve of electrode samples at current 0.1 A $cm^{-2}$: (d) NiFe-($NO_3^-$)-LDH/CC; (e) NiFe-($SO_4^{2-}$)-LDH/CC; (f) NiFe-($CO_3^{2-}$)-LDH/CC.

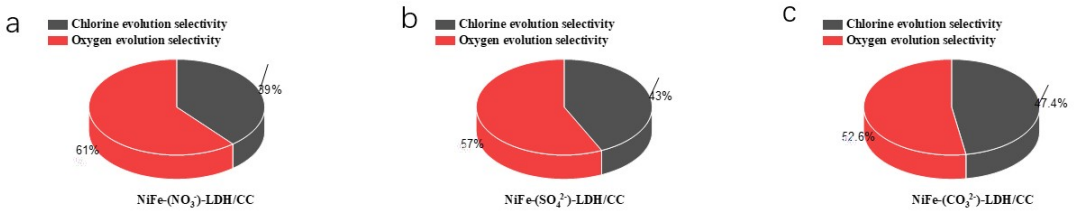


**Figure S8.** Oxygen evolution selectivity of electrode materials in natural seawater on the electrodes at current 0.1 A $cm^{-2}$: (c) NiFe-($NO_3^-$)-LDH/CC; (d) NiFe-($SO_4^{2-}$)-LDH/CC; (e) NiFe-($CO_3^{2-}$)-LDH/CC.

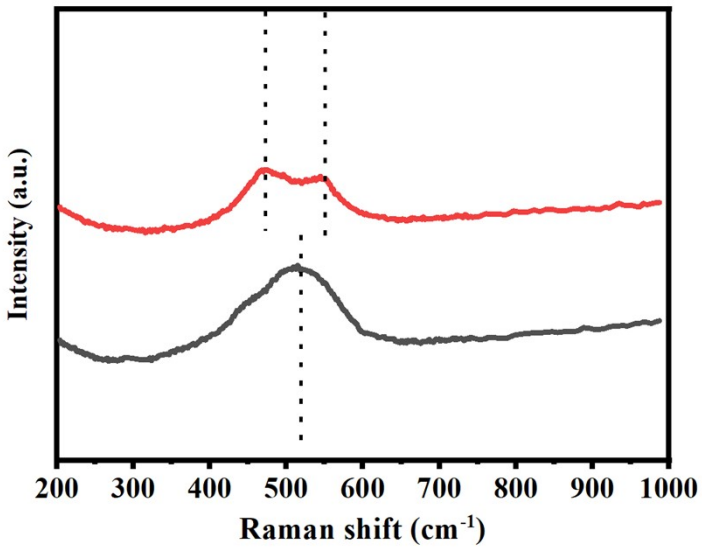


**Figure S9.** Raman shift of the NiFe-($H_2PO_2^-$)-LDH/CC electrode before and after oxidation at 1.45 V vs. RHE.